Nanoscale

ROYAL SOCIETY
OF CHEMISTRY

PAPER
Shengdong Zhang, Shuming Chen *et al.*
Efficient quantum dot light-emitting diodes with a $Zn_{0.85}Mg_{0.15}O$ interfacial modification layer

NCNST

Efficient quantum dot light-emitting diodes with a $Zn_{0.85}Mg_{0.15}O$ interfacial modification layer†

Yizhe Sun,[a] Yibin Jiang,[b] Huiren Peng,[b] Jiangliu Wei,[c] Shengdong Zhang*[a] and Shuming Chen 🆔 *[b]

Efficient inverted quantum-dot (QD) light-emitting diodes (LEDs) are demonstrated by using 15% Mg doped ZnO ($Zn_{0.85}Mg_{0.15}O$) as an interfacial modification layer. By doping Mg into ZnO, the conduction band level, the density of oxygen vacancies and the conductivity of the ZnO can be tuned. To suppress excess electron injection, a 13 nm $Zn_{0.85}Mg_{0.15}O$ interlayer with a relatively higher conduction band edge and lower conductivity is inserted between the ZnO electron transport layer and QD light-emitting layer, which improves the balance of charge injection and blocks the non-radiative pathway. Moreover, according to the electrical and optical studies of devices and materials, quenching sites at the ZnO surface are effectively reduced by Mg-doping. Therefore exciton quenching induced by ZnO nanoparticles is largely suppressed by capping ZnO with $Zn_{0.85}Mg_{0.15}O$. Consequently, the red QLEDs with a $Zn_{0.85}Mg_{0.15}O$ interfacial modification layer exhibit superior performance with a maximum current efficiency of 18.69 cd A^{-1} and a peak external quantum efficiency of 13.57%, which are about 1.72- and 1.74-fold higher than 10.88 cd A^{-1} and 7.81% of the devices without $Zn_{0.85}Mg_{0.15}O$. Similar improvements are also achieved in green QLEDs. Our results indicate that $Zn_{0.85}Mg_{0.15}O$ can serve as an effective interfacial modification layer for suppressing exciton quenching and improving the charge balance of the devices.

1. Introduction

Colloidal quantum dots (QDs) have been attracting increasing attention owing to their properties of tunable emission wavelength, high color purity, high photoluminescence (PL) quantum yield and good stability in the environment.[1–5] Because of these outstanding optoelectronic properties, light-emitting diodes based on QDs (QLEDs) have been the subject of intensive research in recent years. With the rapid development of QD materials and device architectures, the performance of QLEDs is getting closer to that of organic (O) LEDs, thus making them to be one of the promising candidates for next generation displays.[6–10]

In typical QLEDs, ZnO nanoparticles (NPs) are widely used as an electron transport layer (ETL) due to their advantages of high electron mobility, suitable energy level and easy deposition.[11–14] Because of efficient electron injection, highly efficient QLEDs with a low turn on voltage have been

demonstrated.[15–17] For further improving the performance of QLEDs, charge balance should be optimized. This is because in QLEDs, hole injection is relatively inefficient due to the high injection barrier caused by the deep valence level of QDs. The unbalanced hole- and electron-injection charges the QDs and consequently increases the possibility of non-radiative Auger recombination.[18,19] In addition, the interface of ZnO/QD is problematic and has to be modified for further boosting the performance of devices. This is because at the interface of ZnO/QD, excitons are easily quenched by an interfacial charge transfer process and/or by an intragap-assisted non-radiative recombination process.[20,21] The conduction band level of ZnO is well aligned with that of QDs, which facilitates the interfacial charge transfer and thereby promotes the Auger recombination, whereas the intragap states of ZnO, resulting from oxygen vacancies and/or surface defects, act as non-radiative recombination centers and thereby quench the excitons effectively.

A variety of methods have been proposed to improve the charge balance and suppress exciton quenching.[22–27] Among them, the most practical and effective method is inserting an interfacial modification layer (IML) between ZnO and QDs to block the interfacial charge transfer and passivate the intragap states. For instance, Kim *et al.* introduced a polyethylenimine ethoxylated (PEIE) IML for red QLEDs. The application of PEIE reduced the workfunction of ZnO NPs effectively, and thus

[a]Institute of Microelectronics, Peking University, Beijing, 100871, P. R. China. E-mail: zhangsd@pku.edu.cn
[b]Department of Electrical and Electronic Engineering, Southern University of Science and Technology, Shenzhen, 518055, P. R. China. E-mail: chen.sm@sustc.edu.cn
[c]Guangdong Poly Optoelectronics Co., Ltd., Jiangmen, 529040, P. R. China
†Electronic supplementary information (ESI) available. See DOI: 10.1039/c7nr02099f

promoted charge balance and improved current efficiency significantly.[22] In 2014, Peng et al. reported QLEDs with an extremely high external quantum efficiency (EQE) of 20.5% by inserting an insulating poly(methylmethacrylate) (PMMA) layer between ZnO NPs and QDs. The PMMA layer reduced excess electron injection and mitigated the negative impact caused by Auger recombination.[24] In addition, exciton quenching induced by metal oxide was also alleviated. According to Liu's report, a thin polyvinylpyrrolidone (PVP) polymer was employed to passivate the surface of nickel oxide, which enhanced the performance of devices with inhibited efficiency roll-off.[25]

Generally speaking, the adoption of IML is certainly helpful to the improvement of device performance. However, most reported IMLs are based on insulated polymer materials. Considering the relatively insulated property of these materials, the magnitude of current density may be limited. More profoundly, for organic materials, they are highly sensitive to oxygen and moisture, which may deteriorate the lifetime and impede the practical application of QLEDs. In this work, to solve these problems, an inorganic semiconductor based on 15% Mg-doped ZnO ($Zn_{0.85}Mg_{0.15}O$) is adopted as an IML for inverted QLEDs. With a ZnMgO IML, electron injection is significantly alleviated and thus charge balance is effectively improved. Meanwhile, non-radiative recombination centers induced by the defects of ZnO could also be reduced by doping Mg into ZnO. As a consequence, the demonstrated QLEDs with ZnMgO IML exhibit the maximum current efficiency (CE) of 18.69 cd A^{-1} and the peak EQE of 13.57%,

which are about 1.72- and 1.74-fold higher than 10.88 cd A^{-1} and 7.81% of the devices without IML.

2. Results and discussion

ZnMgO NPs were synthesized according to the methods reported in ref. 28. Fig. S1† shows the transmission electron microscopy (TEM) images of the obtained NPs. The diameter of the NPs is about 3–4 nm. The composition of ZnMgO was characterized by X-ray photoelectron spectroscopy (XPS). As shown in Fig. 1(a), for undoped ZnO, the Zn $2p_{3/2}$ peak centered at 1022.4 eV represents the presence of Zn–O bonds. When Mg is doped into ZnO, because of the replacement of Zn^{2+} by Mg^{2+} and the formation of Zn–O–Mg bonds, this peak shifts to a higher binding energy.[29] The inset in Fig. 1(a) shows the Mg 1s spectra of ZnMgO, which also indicates the presence of MgO. By analyzing the atomic concentration of each element, the composition of the NPs was confirmed to be $Zn_{0.85}Mg_{0.15}O$.

The electronic structures of ZnO and ZnMgO NPs were characterized by ultraviolet photon spectroscopy (UPS). Fig. 1(b) and (c) show the UPS spectra of the secondary-electron cutoff and the valence regions of the NPs. Generally, the work function (WF) could be estimated by the difference between the incident light energy (21.2 eV) and the energy of secondary cutoff. In this case, the WF of ZnO NPs and ZnMgO NPs is calculated to be 4.08 eV and 3.69 eV, respectively, as
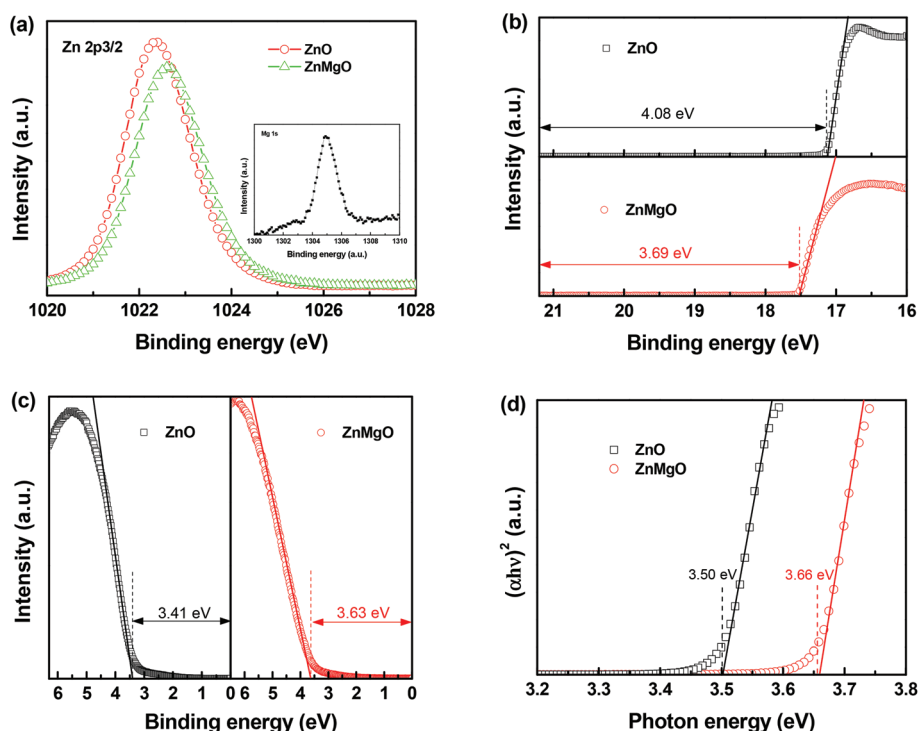

Fig. 1 (a) Zn $2p_{3/2}$ XPS spectra of ZnO and ZnMgO NPs. The inset shows the Mg 1s spectra of ZnMgO. UPS spectra of (b) secondary-electron cutoff and (c) valence-band edge regions of ZnO and ZnMgO films. (d) $(\alpha h\nu)^2 - h\nu$ plots converted from the absorption spectra of ZnO and ZnMgO NPs.

labeled in Fig. 1(b). Compared to ZnO NPs, the lower WF of ZnMgO NPs represents an upward drift in the Fermi level, which is consistent with previous studies.[30,31] In order to define the position of valence band maximum (VBM), the energy gap between the Fermi level and VBM (ΔE_{VB}) is extracted from the valence-band region. As shown in Fig. 1(c), the ΔE_{VB} values of ZnO NPs and ZnMgO NPs are 3.41 eV and 3.63 eV, respectively. As a result, via the summation of WF and ΔE_{VB}, the VBM levels of ZnO and ZnMgO are calculated to be 7.49 eV and 7.32 eV below the vacuum level, respectively. Fig. 1(d) shows the absorption spectra of ZnO NPs and ZnMgO NPs, illustrated as the plots of $(\alpha h\nu)^2$ vs. photon energy $h\nu$, where α is the absorbance. The band gaps (E_g) of these two materials could be determined through the absorption onset of the linear region and the E_g values for ZnO and ZnMgO are found to be 3.50 eV and 3.66 eV, respectively. Therefore, the conduction band minimum (CBM) levels are deduced to be 3.99 eV for ZnO NPs and 3.66 eV for ZnMgO NPs. It is noted that the CBM level of ZnMgO NPs is 0.33 eV higher than that of ZnO NPs. Therefore, considering the aligned CBM between ZnO NPs and QDs (Fig. 2(b)), this energy offset induced by the ZnMgO interlayer could serve as an injection barrier for electrons, which may improve the charge balance and suppress the non-radiative Auger recombination.

To verify our assertion, inverted red QLEDs with the structure ITO/ZnO/ZnMgO/QDs/TcTa/NPB/HATCN/Al were fabricated, where ITO (indium-tin-oxide), ZnO, ZnMgO, QDs, TcTa (4,4′,4″-tris(carbazol-9-yl)triphenylamine), NPB (N,N′-di(naphthalene-1-yl)-N,N′-bis(phenyl)-benzidine), HATCN (dipyrazino[2,3-f:2′,3′-h]quinoxaline-2,3,6,7,10,11-hexacarbonitrile) and Al work as a cathode, ETL, IML, a light emitting layer, an electron blocking layer, a hole transport layer, a hole injection layer and an anode, respectively. The schematic structure and the energy level alignment of the devices are shown in Fig. 2.

To study the effect of ZnMgO thickness on device performance, the thickness of ZnMgO was varied from 0 to 25 nm. As shown in Fig. 3(a), all devices exhibit saturated red emission with a central emission wavelength of 633 nm and a full width at half maximum (FWHM) of 36 nm. Fig. 3(b) shows the current density–voltage–luminance (J–V–L) characteristics of the devices. By doping Mg into ZnO, the conductivity of the resultant ZnMgO is effectively decreased due to the reduction of oxygen vacancies, as will be discussed later. Therefore, devices with ZnMgO IML exhibit reduced current density. Besides, the ZnMgO tends to block the injection of electrons due to its relatively higher CBM. The turn on voltage for the devices with ZnMgO is slightly higher than that of the devices without ZnMgO. However, the luminance for the QLEDs with 7–13 nm ZnMgO is close to that of the control devices especially at a large driving voltage. For example, QLEDs with a 13 nm ZnMgO interlayer exhibit a luminance of 23 590 cd m^{-2} at a driving voltage of 13 V, which is close to 27 290 cd m^{-2} for the reference devices. The comparable luminance obtained at a relatively small current indicates a higher efficiency for the device modified by ZnMgO. Indeed, as shown in Fig. 3(c) and S2,† all devices with ZnMgO IML exhibit significantly increased CE and EQE compared to those of the devices without ZnMgO. Maximum improvement is achieved by using 13 nm ZnMgO. For example, with 13 nm ZnMgO, the CE and EQE are improved from 10.88 cd A^{-1} to 18.69 cd A^{-1}, and from 7.81% to 13.57%, respectively, revealing enhancement factors of 1.72 and 1.74 compared with the reference devices. For devices with thicker ZnMgO IML (25 nm), the performance is deteriorated, which is due to the insufficient carrier injection, as reflected by the extremely low injection current. Similar results are observed in the device with a single ZnMgO ETL as shown in Fig. S3.†

The improvement of efficiency is likely due to the reduction of electron injection, which thus improves the charge balance. To verify this hypothesis, electron-only devices with structures of glass/ITO/ZnO(30 nm)/ZnMgO(10 nm)/QDs/ZnMgO(10 nm)/ZnO(30 nm)/Al and glass/ITO/ZnO(40 nm)/QDs/ZnO(40 nm)/Al were fabricated and their J–V characteristics were measured. To exclude the influence of increased device thickness on J–V characteristics, the total thickness of ZnO/ZnMgO is kept the same as that of ZnO. As shown in Fig. 3(d), devices with ZnMgO IML indeed exhibit a remarkably lower electron current than that of the devices without ZnMgO IML. This is
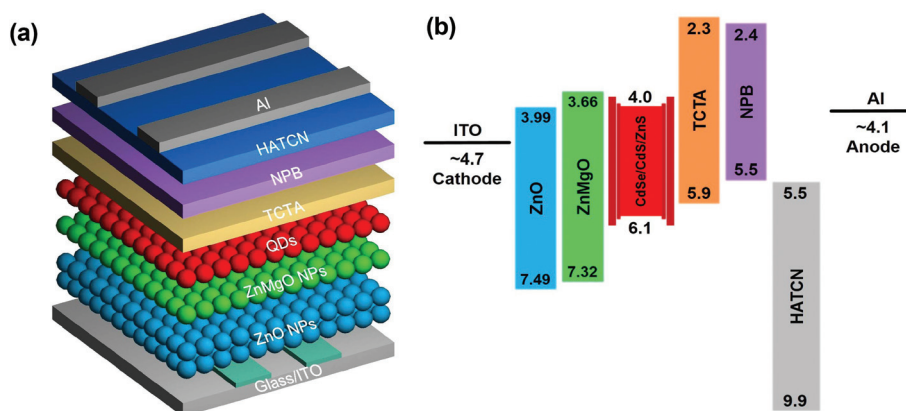

Fig. 2 (a) Schematic structure and (b) energy level alignment of the inverted QLED with a ZnMgO modification layer.
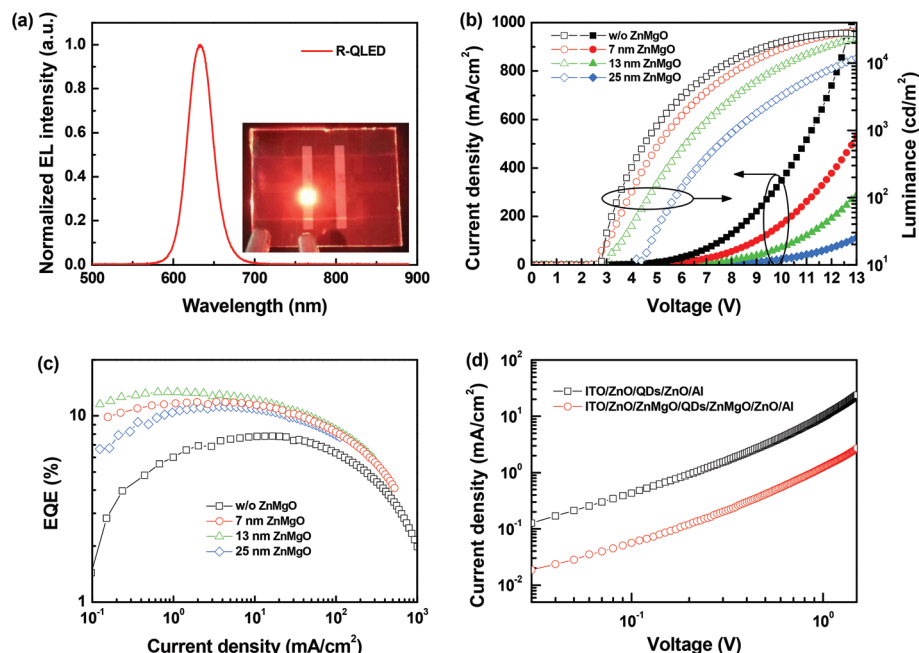
Fig. 3 Device characteristics of the inverted red QLEDs. (a) Normalized EL spectrum of the device. The inset shows the photograph of a device working at 5 V. (b) J−V−L and (c) EQE−J characteristics of the devices with different ZnMgO thickness. (d) J−V characteristics of the electron-only devices with the structures of ITO/ZnO/QDs/ZnO/Al and ITO/ZnO/ZnMgO/QDs/ZnMgO/ZnO/Al.

because the CBM of ZnMgO (3.66 eV) is higher than that (3.99 eV) of ZnO and thus there exists a 0.33 eV injection barrier when electrons are injected from ZnO to ZnMgO. In other words, ZnMgO can effectively block the injection of electrons and thereby reduces the electron current. In addition, the lower conductivity of ZnMgO also contributes to the reduction of electron current. It is known that the conductivity of ZnO is heavily dependent on the amount of oxygen vacancies that generate free carriers and influence the mobility of electrons.[32,33] By doping Mg into ZnO, the concentration of oxygen vacancies can be effectively reduced. This is because the Mg–O bond has a stronger bonding energy (393.7 kJ mol^{-1}) than that of the Zn–O bond (284.1 kJ mol^{-1}).[34] Therefore, it would be much harder to form oxygen vacancies in Mg-doped ZnO NPs. To verify this hypothesis, the chemical bonds of oxygen in ZnO and ZnMgO were characterized by XPS and the resulting O 1s spectra are shown in Fig. 4. The asymmetric O 1s peaks of ZnO and ZnMgO are thoroughly deconvoluted into three Gaussian distributions, which are centered at 529.9 ± 0.1 eV (OI), 531.2 ± 0.1 eV (OII) and 532.0 ± 0.1 eV (OIII), respectively, as shown in Fig. 4(a) and (b). The OI, OII and OIII states are related to the oxygen in oxide lattices, oxygen vacancies and oxygen bonds in the hydroxide, respectively. It is clear that the relative ratio of oxygen vacancies (OII/ OI + OII + OIII) is reduced from 29.6% to 16.9% by doping Mg into ZnO NPs. This result indicates that the oxygen vacancies or loosely bonded oxygen states are effectively reduced by the Mg doping and this leads to the lower conductivity of ZnMgO compared to ZnO. To conclude, the reduction of electron current in devices with ZnMgO IML is due to: (1) the
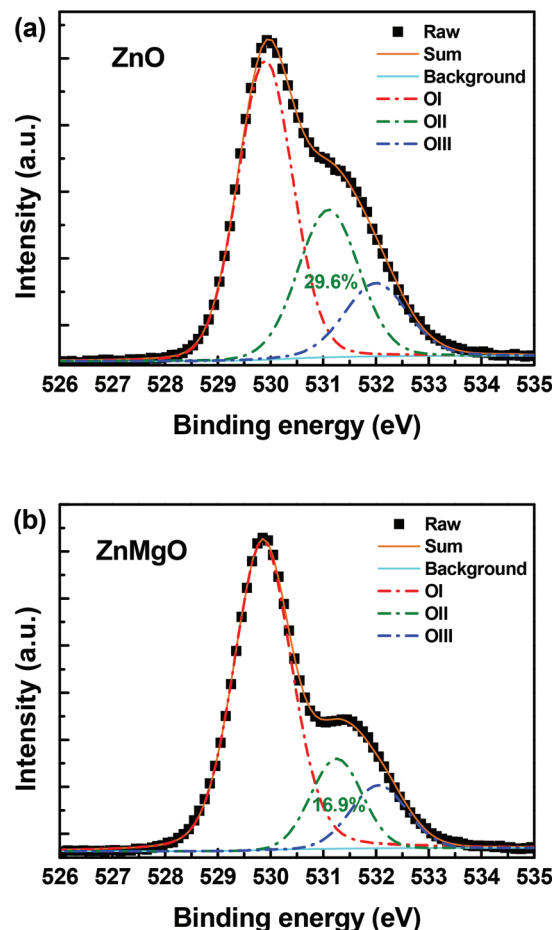

Fig. 4 The O 1s XPS spectra of (a) ZnO and (b) ZnMgO films.

higher CBM level of ZnMgO which induces an extra energy barrier for the injection of electrons and (2) the lower conductivity of ZnMgO which slows down the pace of electron transport.

The improvement of efficiency is also due to the suppression of exciton quenching. Fig. 5(a) and (b) show the steady and time-resolved PL spectra of three samples with structures of glass/QDs, glass/ZnO/QDs and glass/ZnO/ZnMgO/QDs. As can be seen, the PL intensity and exciton lifetime of QDs drop significantly when they are directly in contact with ZnO. This is because at the ZnO/QD interface, excitons are easily quenched by an interfacial charge transfer process, and/or by an intragap-assisted non-radiative recombination process. However, by inserting a ZnMgO IML between ZnO and QDs, the PL intensity and the exciton lifetime are enhanced greatly, which indicates that with ZnMgO IML, both quenching processes can be effectively suppressed. This is because the higher CBM level of ZnMgO blocks the interfacial charge transfer, whereas the lower intragap concentration alleviates the non-radiative recombination. The intragap states of metal oxide usually originate from the defects such as oxygen vacancies that could be ionized into positively charged states (V_O^+, V_O^{++}) or maintain electric neutrality (V_O).[14] To examine the defect concentration of ZnO and ZnMgO, the PL spectra of both materials in solution were measured. As shown in Fig. 5(c), the PL spectra exhibit two emission peaks which correspond to a sharp band-edge ultraviolet emission and a broad visible emission, respectively. The visible emission orig-

inate from the recombination of the electrons trapped by the shallow donor level near the conduction band-edge with the holes trapped at the intragap states, and therefore the intensity of visible emission reflects the concentration of defects. It is found that the peak of visible emission is blue-shifted from 558.5 nm for ZnO NPs to 536.8 nm for ZnMgO NPs due to the increasing band gap induced by Mg doping. Additionally, the defect emission is suppressed remarkably while the band-edge emission is promoted significantly by the Mg doping. The diminished visible emission can be attributed to the reduction of oxygen vacancies owing to the stronger bonding between Mg and O, which is well consistent with the above XPS spectra where oxygen vacancies are verified to be fewer in the ZnMgO film. Based on earlier research, the intragap states located inside the bandgap of ZnO could act as charge recombination sites, which trap holes and quench excitons due to the well-aligned defect level with the VBM of QDs.[35,36] Therefore, the introduction of ZnMgO IML could provide a preferable interface with fewer intragaps or quenching sites. This process is briefly illustrated in Fig. 5(d). To conclude, due to the reduced defect concentration of ZnMgO, exciton quenching can be effectively suppressed and thus the efficiency of red QLEDs is significantly improved by using the ZnMgO IML.

To verify if the ZnMgO IML could be applied in full color devices, inverted green and blue QLEDs were also fabricated and tested. Their EL spectra are shown in Fig. S4.† The device performance of green and blue devices is shown in Fig. S5.† For the green QLEDs with ZnMgO modification layer, although
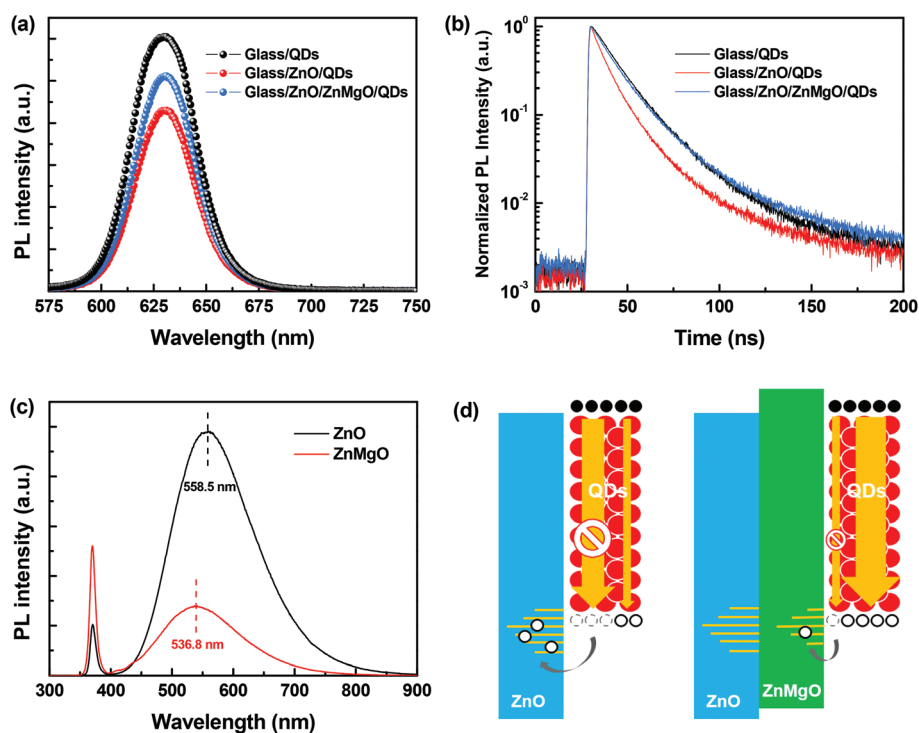

Fig. 5 (a) PL spectra and (b) time-resolved PL spectra of different samples, glass/QDs, glass/ZnO/QDs, and glass/ZnMgO/QDs. (c) PL spectra of ZnO NPs and ZnMgO NPs. (d) Illustrated scheme for exciton quenching induced by metal oxide NPs. The quenching process can be effectively suppressed by inserting ZnMgO between ZnO and QDs.

the current density is lower than that of the reference devices, their luminance reaches to a similar level at about 10 V, implying a higher current efficiency. This is confirmed by the CE–J characteristic as shown in Fig. S5(b).† Green QLEDs exhibit improved CE from 21.65 cd A^{-1} to 29.64 cd A^{-1}, representing a 1.37-fold enhancement by the adoption of the ZnMgO layer. The improved efficiency could be attributed to the superior interface between ZnMgO and QDs rather than the suppression of Auger recombination because of the higher CBM level of green QDs. However, blue QLEDs exhibit deteriorated performance when the ZnMgO interlayer is applied. The remarkable positive shift of turn-on voltage implies that ZnMgO hinders the injection of electrons significantly.

3.   Conclusions

In conclusion, by utilizing a ZnMgO IML, inverted red QLEDs with high efficiency have been developed. The ZnMgO IML plays dual roles in the improved device performance. On the one hand, the relatively resistive ZnMgO layer introduces an extra energy barrier for electron injection and thus reduces the injection of excess electrons. This result contributes to the balanced carrier injection and thus improves the device efficiency. On the other hand, recombination sites induced by oxygen vacancy related defects are effectively reduced by Mg doping, and thus exciton quenching caused by intragap-induced recombination is effectively suppressed by using the ZnMgO IML. As a result, the maximum CE and peak EQE of the red QLEDs reach 18.69 cd A^{-1} and 13.57%, respectively. These values are about 1.72- and 1.74-fold higher than those of the devices without ZnMgO. Furthermore, the ZnMgO IML is also applied in green and blue inverted devices. These experimental results suggest that the use of the ZnMgO modification layer is a promising way to realize high-performance inverted QLEDs for next generation display and lighting applications.

4.   Experimental section

4.1   Synthesis of ZnMgO nanoparticles

Colloidal Mg-doped ZnO nanocrystals were synthesized by the reported method under ambient conditions with some modification.[28] For a typical synthesis of the $Zn_{0.85}Mg_{0.15}O$ solution, an ethanol solution of potassium hydroxide (0.4 mol L^{-1}) was dropwise added into a three-neck flask, in which 17 mmol zinc acetate dehydrate and 3 mmol magnesium acetate were dissolved in a mixture of 120 mL dimethyl sulfoxide and 120 mL ethanol previously. The solution was kept stirring vigorously for 3 hours after the end of dropwise addition, and then Mg-doped ZnO nanoparticles were washed and redispersed by using ethyl acetate and ethanol, respectively. Addition of ethanolamine was introduced to stabilize the nanoparticles. The sample was finally stored in absolute ethanol.

4.2.   QLED fabrication

Inverted QLEDs with a structure of glass/ITO/ZnO (25 nm)/ ZnMgO/QDs/TcTa (20 nm)/NPB (40 nm)/HATCN (10 nm)/Al were fabricated. For comparison, devices without ZnMgO modification were also prepared. ZnO NPs were spin-coated at 1500 rpm onto the pre-cleaned substrate from a 20 mg mL^{-1} butanol solution, followed by baking at 120 °C for 20 min. After that, 15% Mg-doped ZnO NPs dissolved in ethanol were spin-coated at 5000 rpm onto the ZnO layer and then annealed at 110 °C for 15 min. To investigate the impact of ZnMgO thickness on device performance, the concentration of the ZnMgO solution was varied from 5 to 15 to 25 mg mL^{-1}. The red CdSe/CdS/ZnS/oleic acid (core/ shell/ligand) QDs purchased from Guangdong Poly OptoElectronics Co., Ltd with an emission wavelength of 630 nm and a PL quantum yield of 82.7% were dissolved in n-octane with a concentration of 20 mg mL^{-1} and then spin-coated at 1500 rpm for 45 s, followed by annealing at 100 °C for 5 min. Besides, the green and blue QDs applied in our devices were also commercially available from Mesolight Inc. and Guangdong Poly OptoElectronics Co., Ltd with the structure of CdZnSeS/ZnS/oleic acid (core/shell/ligand) and ZnCdS/ZnS/oleic acid (core/shell/ligand), respectively. The green QDs were spin-coated from a 5 mg mL^{-1} hexane solution at 2000 rpm for 45 s. The blue QDs were spin-coated from a 10 mg mL^{-1} toluene solution at 1500 rpm for 45 s. All layers fabricated by the spin-coating method are deposited in a N_2-filled glove box. Subsequently, other functional layers were thermally evaporated in a vacuum evaporator with a base pressure of 5×10^{-4} Pa.

4.3   Characterization

The thicknesses of the solution processed films were measured using a Bruker DektakXT Stylus Profiler, while the thicknesses of ZnMgO less than 20 nm were estimated by an absorbance-thickness method (Fig. S6†) that assumed a linear dependence of the absorbance at 330 nm on thickness and calculated to be 13 nm and 7 nm corresponding to solution concentrations of 15 mg mL^{-1} and 5 mg mL^{-1}, respectively. The current density–luminance–voltage (J–V–L) characteristics were measured by a dual-channel Keithley 2614B source measure unit and a PIN-25D silicon photodiode. The electroluminescence (EL) spectra of QLEDs were measured by using a fiber optic spectrometer (Ocean Optics USB 2000) in the normal direction. The active area of the devices was 2 mm × 2 mm. All measurements were performed in air at room temperature. Measurements of the absorbance and photoluminescence (PL) spectra of ZnO and ZnMgO NPs were carried out with a scanning monochromator (Ocean Optics MonoScan 2000). The PL and time-resolved PL (TRPL) spectra of the samples fabricated on quartz substrates were measured by using an Edinburgh instruments FLS980 spectrometer. The UPS and XPS results of ZnO and ZnMgO films were obtained using a Kratos Axis Ultra DLD.

Acknowledgements

References

1 Y. Yin and A. P. Alivisatos, Colloidal Nanocrystal Synthesis and the Organic-Inorganic Interface, *Nature*, 2005, **437**, 664–670.

2 S. Coe, W. K. Woo, M. Bawendi and V. Bulovic, Electroluminescence from Single Monolayers of Nanocrystals in Molecular Organic Devices, *Nature*, 2002, **420**, 800–803.

3 X. Y. Yang, D. W. Zhao, K. S. Leck, S. T. Tan, Y. X. Tang, J. L. Zhao, H. V. Demir and X. W. Sun, Full Visible Range Covering InP/ZnS Nanocrystals with High Photometric Performance and Their Application to White Quantum Dot Light-Emitting Diodes, *Adv. Mater.*, 2012, **24**, 4180–4185.

4 V. L. Colvin, M. C. Schlamp and A. P. Alivisatos, Light-Emitting-Diodes Made from Cadmium Selenide Nanocrystals and a Semiconducting Polymer, *Nature*, 1994, **370**, 354–357.

5 D. Bozyigit and V. Wood, Challenges and Solutions for High-Efficiency Quantum Dot-Based LEDs, *MRS Bull.*, 2013, **38**, 731–736.

6 Q. Sun, Y. A. Wang, L. S. Li, D. Wang, T. Zhu, J. Xu, C. Yang and Y. Li, Bright, Multicoloured Light-Emitting Diodes Based on Quantum Dots, *Nat. Photonics*, 2007, **1**, 717–722.

7 K. H. Lee, J. H. Lee, H. D. Kang, B. Park, Y. Kwon, H. Ko, C. Lee, J. Lee and H. Yang, Over 40 cd/A Efficient Green Quantum Dot Electroluminescent Device Comprising Uniquely Large-Sized Quantum Dots, *ACS Nano*, 2014, **8**, 4893–4901.

8 J. Lim, M. Park, W. K. Bae, D. Lee, S. Lee, C. Lee and K. Char, Highly Efficient Cadmium-Free Quantum Dot Light-Emitting Diodes Enabled by the Direct Formation of Excitons within InP@ZnSeS Quantum Dots, *ACS Nano*, 2013, **7**, 9019–9026.

9 H. B. Shen, S. Wang, H. Z. Wang, J. Z. Niu, L. Qian, Y. X. Yang, A. Titov, J. Hyvonen, Y. Zheng and L. S. Li, Highly Efficient Blue-Green Quantum Dot Light-Emitting Diodes Using Stable Low-Cadmium Quaternary-Alloy ZnCdSSe/ZnS Core/Shell Nanocrystals, *ACS Appl. Mater. Interfaces*, 2013, **5**, 4260–4265.

10 Y. X. Yang, Y. Zheng, W. R. Cao, A. Titov, J. Hyvonen, J. R. Manders, J. G. Xue, P. H. Holloway and L. Qian, High-Efficiency Light-Emitting Devices Based on Quantum Dots with Tailored Nanostructures, *Nat. Photonics*, 2015, **9**, 259–266.

11 L. Qian, Y. Zheng, J. Xue and P. H. Holloway, Stable and Efficient Quantum-Dot Light-Emitting Diodes Based on Solution-Processed Multilayer Structures, *Nat. Photonics*, 2011, **5**, 543–548.

12 J. H. Kim, K. H. Lee, H. D. Kang, B. Park, J. Y. Hwang, H. S. Jang, Y. R. Do and H. Yang, Fabrication of a White Electroluminescent Device Based on Bilayered Yellow and Blue Quantum Dots, *Nanoscale*, 2015, **7**, 5363–5370.

13 K. H. Lee, C. Y. Han, H. D. Kang, H. Ko, C. Lee, J. Lee, N. Myoung, S. Y. Yim and H. Yang, Highly Efficient, Color-Reproducible Full-Color Electroluminescent Devices Based on Red/Green/Blue Quantum Dot-Mixed Multilayer, *ACS Nano*, 2015, **9**, 10941–10949.

14 B. S. Mashford, M. Stevenson, Z. Popovic, C. Hamilton, Z. Zhou, C. Breen, J. Steckel, V. Bulovic, M. Bawendi, S. Coe-Sullivan and P. T. Kazlas, High-Efficiency Quantum-Dot Light-Emitting Devices with Enhanced Charge Injection, *Nat. Photonics*, 2013, **7**, 407–412.

15 Y. Shirasaki, G. J. Supran, M. G. Bawendi and V. Bulovic, Emergence of Colloidal Quantum-Dot Light-Emitting Technologies, *Nat. Photonics*, 2013, **7**, 13–23.

16 J. Kwak, W. K. Bae, D. Lee, I. Park, J. Lim, M. Park, H. Cho, H. Woo, D. Y. Yoon, K. Char, S. Lee and C. Lee, Bright and Efficient Full-Color Colloidal Quantum Dot Light-Emitting Diodes Using an Inverted Device Structure, *Nano Lett.*, 2012, **12**, 2362–2366.

17 H. Zhang, H. R. Li, X. W. Sun and S. M. Chen, Inverted Quantum-Dot Light-Emitting Diodes Fabricated by All-Solution Processing, *ACS Appl. Mater. Interfaces*, 2016, **8**, 5493–5498.

18 W. K. Bae, S. Brovelli and V. I. Klimov, Spectroscopic Insights into the Performance of Quantum Dot Light-Emitting Diodes, *MRS Bull.*, 2013, **38**, 721–730.

19 W. K. Bae, Y. S. Park, J. Lim, D. Lee, L. A. Padilha, H. McDaniel, I. Robel, C. Lee, J. M. Pietryga and V. I. Klimov, Controlling the Influence of Auger Recombination on the Performance of Quantum-Dot Light-Emitting Diodes, *Nat. Commun.*, 2013, **4**, 2661.

20 K. Tvrdy, P. A. Frantsuzov and P. V. Kamat, Photoinduced Electron Transfer from Semiconductor Quantum Dots to Metal Oxide Nanoparticles, *Proc. Natl. Acad. Sci. U. S. A.*, 2011, **108**, 29–34.

21 W. H. Cheng, J. W. Chiou, M. Y. Tsai, J. S. Jeng, J. S. Chen, S. L. C. Hsu and W. Y. Chou, Lithium-Induced Defect Levels in ZnO Nanoparticles To Facilitate Electron Transport in Inverted Organic Photovoltaics, *J. Phys. Chem. C*, 2016, **120**, 15035–15041.

22 H. H. Kim, S. Park, Y. Yi, D. I. Son, C. Park, D. K. Hwang and W. K. Choi, Inverted Quantum Dot Light Emitting Diodes Using Polyethylenimine Ethoxylated Modified ZnO, *Sci. Rep.*, 2015, **5**, 8968.

23 H. Zhang, N. Sui, X. C. Chi, Y. H. Wang, Q. H. Liu, H. Z. Zhang and W. Y. Ji, Ultrastable Quantum-Dot Light-Emitting Diodes by Suppression of Leakage Current and Exciton Quenching Processes, *ACS Appl. Mater. Interfaces*, 2016, **8**, 31385–31391.

24 X. L. Dai, Z. X. Zhang, Y. Z. Jin, Y. Niu, H. J. Cao, X. Y. Liang, L. W. Chen, J. P. Wang and X. G. Peng,

Solution-Processed, High-Performance Light-Emitting Diodes Based on Quantum Dots, *Nature*, 2014, **515**, 96–99.

25 S. Liu, S. Ho, Y. Chen and F. So, Passivation of Metal Oxide Surfaces for High-Performance Organic and Hybrid Optoelectronic Devices, *Chem. Mater.*, 2015, **27**, 2532–2539.

26 H. M. Kim, A. B. Yusoff, J. H. Youn and J. Jang, Inverted Quantum-Dot Light Emitting Diodes with Cesium Carbonate Doped Aluminium-Zinc-Oxide as the Cathode Buffer Layer for High Brightness, *J. Mater. Chem. C*, 2013, **1**, 3924–3930.

27 N. Kirkwood, B. Singh and P. Mulvaney, Enhancing Quantum Dot LED Efficiency by Tuning Electron Mobility in the ZnO Electron Transport Layer, *Adv. Mater. Interfaces*, 2016, **3**, 1600868.

28 E. A. Meulenkamp, Synthesis and Growth of ZnO Nanoparticles, *J. Phys. Chem. B*, 1998, **102**, 5566–5572.

29 L. Q. Jing, Z. L. Xu, J. Shang, X. J. Sun, W. M. Cai and H. C. Guo, The Preparation and Characterization of ZnO Ultrafine Particles, *Mater. Sci. Eng., A*, 2002, **332**, 356–361.

30 D. C. Olson, S. E. Shaheen, M. S. White, W. J. Mitchell, M. F. A. M. van Hest, R. T. Collins and D. S. Ginley, Band-Offset Engineering for Enhanced Open-Circuit Voltage in Polymer-Oxide Hybrid Solar Cells, *Adv. Funct. Mater.*, 2007, **17**, 264–269.

31 J. H. Kim, C. Y. Han, K. H. Lee, K. S. An, W. Song, J. Kim, M. S. Oh, Y. R. Do and H. Yang, Performance Improvement of Quantum Dot-Light-Emitting Diodes Enabled by an Alloyed ZnMgO Nanoparticle Electron Transport Layer, *Chem. Mater.*, 2015, **27**, 197–204.

32 K. Nomura, H. Ohta, A. Takagi, T. Kamiya, M. Hirano and H. Hosono, Room-Temperature Fabrication of Transparent Flexible Thin-Film Transistors Using Amorphous Oxide Semiconductors, *Nature*, 2004, **432**, 488–492.

33 E. Fortunato, P. Barquinha and R. Martins, Oxide Semiconductor Thin-Film Transistors: A Review of Recent Advances, *Adv. Mater.*, 2012, **24**, 2945–2986.

34 C. J. Ku, W. C. Hong, T. Mohsin, R. Li, Z. Q. Duan and Y. C. Lu, Improvement of Negative Bias Stress Stability in $Mg_{0.03}Zn_{0.97}O$ Thin-Film Transistors, *IEEE Electron Device Lett.*, 2015, **36**, 914–916.

35 E. Polydorou, A. Zeniou, D. Tsikritzis, A. Soultati, I. Sakellis, S. Gardelis, T. A. Papadopoulos, J. Briscoe, L. C. Palilis, S. Kennou, E. Gogolides, P. Argitis, D. Davazoglou and M. Vasilopoulou, Surface Passivation Effect by Fluorine Plasma Treatment on ZnO for Efficiency and Lifetime Improvement of Inverted Polymer Solar Cells, *J. Mater. Chem. A*, 2016, **4**, 11844–11858.

36 J. Mei, M. S. Bradley and V. Bulović, Photoluminescence Quenching of Tris-(8-Hydroxyquinoline) Aluminum Thin Films at Interfaces with Metal Oxide Films of Different Conductivities, *Phys. Rev. B: Condens. Matter*, 2009, **79**, 235205.